The final publication is available at

http://doi.org/10.1038/s41929-018-0104-7

Additional Information

**Synthesis of reaction-adapted zeolite catalysts for MTO with mimics of reaction intermediates as OSDAs. An enzymatic behavior of zeolites.**

Chengeng Li,[+] Cecilia Paris,[+] Joaquín Martínez-Triguero, Mercedes Boronat, Manuel Moliner, Avelino Corma*

Instituto de Tecnología Química, Universitat Politècnica de València-Consejo Superior de Investigaciones Científicas, Avenida de los Naranjos s/n, 46022 València, Spain

*Corresponding author:  E-mail addresses: acorma@itq.upv.es

[+] These authors have contributed equally

1

**Abstract**

Catalysis with enzymes and zeolites have in common the presence of well-defined single active sites, as well as the presence of pockets or cavities in where the transition state of the reaction can be stabilized by means of longer range interactions. We show here that for a complex reaction such as the conversion of methanol to olefins (MTO), it is possible to synthesize reaction-adapted zeolites by using mimics of the key molecular species involved in the molecular mechanism of MTO. The effort has been concentrated on the intermediates of the paring mechanism since the paring is less favored energetically than the side chain route. All the OSDAs based on mimics of the reaction intermediate molecules, exclusively crystallize cage-based small pore zeolitic materials in the aluminosilicate or the silicoaluminophosphate (SAPO) forms, being all of them adequate to perform the MTO reaction. Among the zeolite structures obtained, RTH is the one that favors the most the whole reaction steps following the paring route and, gives the highest $C_3^=/C_2^=$ and $C_4^=/C_2^=$ ratio in the products.

**Keywords**

2

## INTRODUCTION

The methanol-to-olefins (MTO) is a commercial process that produces light olefins ($C_2^=$-$C_5^=$) from synthesis gas via methanol, using zeolite-based catalysts.[1, 2] While methanol is obtained today from synthesis gas derived from natural gas and coal, it is expected that in a future energy scenario, in which abundant and inexpensive $H_2$ will be obtained from water, methanol will be a key molecule to store $H_2$, as well as to produce olefins and aromatics for chemicals. Despite the MTO technology has been successfully implemented, the mechanism of the reactions involved is not yet fully understood. This is due to the complexity of the process, and the fact that the product distribution and coke formation strongly depend on zeolite structure and reaction conditions.[3, 4] There is however a general consensus that the MTO reaction proceeds through an indirect "hydrocarbon pool (HP) mechanism", according to which organic species initially formed from methanol during an induction period and confined within the zeolite channels and cavities, act as co-catalysts for the reaction.[5-11] These HP species are repeatedly methylated by methanol or dimethylether and subsequently split off light alkenes. In fact, the HP species, i.e. aromatic polymethylbenzenes (PMBs) and their corresponding carbenium ions (MB⁺),[5, 12] as well as polymethylcyclopentenyl (MCP⁺) cations,[13, 14] have been detected by in situ ¹³C MAS NMR spectroscopy using isotopically-labelled methanol in different zeolites, and have been proposed as the main components of the hydrocarbon pool in H-SAPO-34, H-BEA and H-ZSM-5 catalysts.

Two competitive routes have been presented as possible pathways according to the HP mechanism, i.e. the side-chain [15, 16] and the paring routes (see Figure 1).[17] The side-chain path proceeds via the alkylation of the polymethylbenzene-related intermediates with methanol, followed by side-chain elimination to form the light olefins, preferentially ethylene and propylene.[5, 12] The paring cycle comprises an initial contraction of the polymethylbenzenium cations (MB⁺), followed by the expansion of polymethylcyclopentenyl cations (MCP⁺), resulting in

3

the preferential formation of propylene.(*10, 13, 17*) The experimental observation of the two types of cations, MB$^+$ and MCP$^+$, by in situ techniques indicate the feasibility of pathways during the MTO process.(*13, 14*) However, the lower energy-barriers calculated for the side-chain mechanism in H-ZSM-5 suggest that the light olefins would be preferentially achieved through aromatic side-chain alkylations.(*10*)

It has been described in the literature that when small pore zeolites containing cavities in their structure are used in the MTO reaction, the product selectivity towards different light olefins as well as the catalyst lifetime are influenced by the framework structure.(*18*) That observation could be explained by the ability of the cavities present in the zeolite to favor the formation of different polyalkylated aromatics depending on their size/shape. In general, small pore zeolites with very large cavities [i.e. zeolite AFX: 15.9x10.4 Å] would favor an excessive alkylation of the aromatic HP species resulting in a faster catalyst deactivation by coke formation, whereas very small cavities [i.e. zeolite LEV: 9.8x9.5 Å] would mostly preclude the HP reaction mechanisms, limiting their catalytic activity.(*19*) On the other hand, different small pore zeolite structures containing cavities with intermediate sizes, though prepared with similar crystal sizes and chemical compositions, present different selectivities towards ethylene and propylene.(*20-24*) For instance, the high-silica SSZ-39 (AEI, cage dimensions: 12.6x11.2 Å) and RUB-13 (RTH, cage dimensions: 11.6x10.0 Å) zeolites tend to give higher propylene/ethylene ratio compared to high-silica CHA (cage dimensions: 11.7x10.2 Å) zeolite (see Figure S1),(*20, 22*) though the size of the pores and cavities, especially in the case of RTH and CHA, are very close. According to these results, it could be envisioned that even small differences in the zeolite cages may stabilize in a different manner the formation of the HP aromatic intermediates shown in Figure 1, favoring the side chain or the paring mechanism, and changing in that way the selectivity within the olefins obtained.

If this is so, it seems reasonable that if one was able to design the cage cavity within the small pore zeolite with the adequate size and/or shape for maximizing the stabilization of particular HP intermediates, the catalyst lifetime and/or the preferential selectivity towards specific light olefins could also be maximized. In this sense, we have very recently described a new ab-initio zeolite synthesis methodology based on the use of organic structure directing agents (OSDAs) that mimic the transition states of some preestablished chemical reactions. The objective was that these mimic OSDAs could drive the synthesis towards adequate zeolite structures to catalyze the preestablished chemical reactions.(*25*) Following this strategy, different zeolite structures were synthesized that improved the activity and/or the selectivity to target products for different industrially-relevant chemical reactions.(*25*)

We propose here that the synthesis of zeolite-based MTO catalysts could be carried out using mimics of the HP intermediates as OSDAs. Then, if this was successful, the crystallization of zeolites presenting adjusted cages for maximizing the host-guest interactions between the inorganic framework and the polyalkylated aromatic MTO intermediates could be achieved, and olefin selectivity could be influenced. It would be of special interest if one could, in this way, direct the reaction towards the energetically less favorable paring route, which should give a higher selectivity to the most desired propylene versus ethylene.

**RESULTS AND DISCUSSION**

According to previous theoretical studies on the MTO process (*8, 10, 13*), and our own DFT calculations presented in the Supporting Information (Figures S2-S5), the paring route starts with a ring contraction of the polymethylbenzenium ($MB^+$) cation to form either a isopropyl-alkylated intermediate (see INT1a in Figure 1 and INT1 in Figure S2) or a polyalkylated bicyclic intermediate (see INT1b in Figure 1 and INT1 in Figure S3), that splits off propene generating a

5

polymethylcyclopentenyl (MCP$^+$) cation (INT3 in Figure 1, S2 and S3). It has also been proposed that a second isomerization of INT1 via INT2 can produce isobutene and a less substituted MCP$^+$ cation in two steps (see Figures S2 and S3). After olefin release there is a ring expansion of the MCP$^+$ intermediate INT3 that, in two steps, is converted into a low-alkylated MB$^+$ cation (INT5 in Figure 1 and S5) which is further alkylated by two methanol molecules regenerating the initial HP species and the reaction cycle starts again.

Following the described ab-initio mimicking approach for the synthesis of reaction-adapted zeolites, we have first prepared a series of OSDAs (see Figure 2a) that mimic the key molecular species involved in the paring mechanism, i.e. INT1, INT3 and INT5. In principle, if the above OSDAs were able to crystallize small pore zeolites, they should maximize interactions between the organic molecules and the walls within the zeolite cavity. Then, the zeolite or zeolites synthesized should minimize the energy for the formation of the molecular species involved in the paring mechanism and, accordingly, increase the $C_3^=/C_2^=$ ratio.

Taking the isopropyl alkylated or the polyalkylated bicyclic HP intermediates (see INT1a and INT1b, respectively, in Figure 1) as possible candidates involved in the ring contraction step of the paring cycle, we carried out the preparation of two OSDAs, i.e. OSDA1a and OSDA1b (see Figure 2a) as mimics. Then, a zeolite synthesis phase diagram was considered (see Figures S6 and S7) with the following synthesis variables: Si/Al [6-15], OSDA/Si [0.2-0.4], NaOH/Si [0-0.2], H$_2$O/Si [3-20], and P/Al [0.8-0.9] ratios, together with the use of different sources of Si, Al, or P (see experimental). In this way, the directing effects of the OSDAs towards the crystallization of zeolites (silicoaluminates) or related-zeotypes (i.e. silicoaluminophosphates, SAPOs) was studied.

Interestingly, the silicoaluminate form of the CHA zeolite, SSZ-13, was obtained using OSDA1a and OSDA1b (see Figures S6 and S7). In the case of OSDA1a, the SSZ-13 material was crystallized only under very specific synthesis conditions (Si/Al=6, see SSZ-13 in Figure S6). Furthermore, it should

be noted that the CHA-related zeolite is the sole microporous material obtained within all the synthesis conditions studied. In contrast, OSDA1b allows the selective crystallization of SSZ-13 zeolite under broader synthesis conditions, revealing the excellent organic directing role of the OSDA1 towards the crystallization of CHA-related zeolites (see Figure S7). The PXRD patterns of the as-prepared SSZ-13_OSDA1a and SSZ-13_OSDA1b materials confirm the crystallization of CHA as pure crystalline phase in both cases (see in Figure S10). Elemental analyses reveal that the organic molecules remain intact within the crystallized products (see Table S2). The calcined SSZ-13 materials show similar textural properties compared to other CHA-related zeolites reported previously in the literature (micropore volume ~0.22-0.25 $cm^3$/g), and the chemical analysis indicate that the final Si/Al molar ratios are comparable to the initial Si/Al molar ratios introduced in the synthesis gels (~6 and ~15 for the SSZ-13_OSDA1a and SSZ-13_OSDA1b, respectively, see Table S3). These two samples have also been studied by FE-SEM microscopy, observing that the SSZ-13_OSDA1a and SSZ-13_OSDA1b show average crystal sizes of ~200-400 nm and ~60-80 nm, respectively (see Figure S11).

At this point, we decided to measure the catalytic activity and selectivity of the SSZ-13 zeolites obtained and compare with those reported in the literature for the conversion of methanol into olefins. Thus, from the different SSZ-13 samples obtained with OSDA1b, we selected one sample with a Si/Al ratio of 15 (see SSZ-13 in Figure S7), since the "standard" SSZ-13 reported in the literature synthesized using N,N,N-trimethyladamantammonium (TMAda) as OSDA is usually prepared with that Si/Al molar ratio.(*26, 27*)

The catalytic activity of these SSZ-13 zeolites has been evaluated for the MTO reaction at 350°C with a WSHV of 0.8 $h^{-1}$. For comparison purposes, a standard SSZ-13 zeolite has been prepared (see physico-chemical properties for the SSZ-13_std in Table S3). However, since the crystal size of our SSZ-13_OSDA1b is very small, a nanosized SSZ-13 has also been prepared for a fair

7

comparison. The nanosized SSZ-13 was prepared by combining the use of TMAda and a surfactant molecule (cetyltrimethylammonium, CTMA) as OSDAs (see physico-chemical properties for the SSZ-13_nano in Table S3).(27) As seen in Table 1, the catalytic lifetime of the SSZ-13_OSDA1a zeolite is remarkably lower than the observed for the SSZ-13_std, due to the lower Si/Al molar ratio of the former (Si/Al=6).(23) However, the SSZ-13_OSDA1b zeolite presents comparable Si/Al molar ratios (Si/Al=15) to other related-CHA zeolites used previously in the literature for the MTO reaction, as it is the case of the SSZ-13_std and SSZ-13_nano.(27) As shown in Figure 3, the SSZ-13_OSDA1b zeolite shows a very important increase of the catalyst lifetime compared not only to the "standard" SSZ-13 catalyst, which presents larger crystal size, but also compared to the SSZ-13 with nanosized crystallites (see Figure 3). In fact, the dropping of methanol conversion below 95% is obtained at ~1000 min time on stream for the SSZ-13 catalyst synthesized using the mimic OSDA1b, whereas for the standard SSZ-13 and the surfactant-based nanosized SSZ-13 materials are 212 and 472 min, respectively (see Table 1). These results highlight the importance of using a mimic OSDA of the HP intermediates for synthesizing a very active and stable CHA-related MTO catalyst compared to other similar SSZ-13 catalysts synthesized with the TMAda catalyst.

The second step of the paring mechanism is the formation of the pentaMCP$^+$ intermediate cation (see INT3 in Figure 1), accompanied by the formation of a molecule of propylene. According to this, we propose a pentamethylimidazolium cation as potential mimic of the pentaMCP$^+$ intermediate (see OSDA3 in Figure 2a). Most interestingly, the use of OSDA3 resulted in the preferential crystallization of the RUB-13 (RTH structure, 8x8-rings) and STA-6 (SAS structure, 8-rings) when the syntheses of silicoaluminates or silicoaluminophosphates were respectively attempted (see Figure S8). These results show the high specificity of this organic molecule towards these small-pore crystalline frameworks, both containing the presence of large cavities within their structures.

In the case of the RUB-13, we have selected a sample synthesized with a Si/Al molar ratio of ~16 (see RUB-13 in Figure S8) for further comparisons with the above described SSZ-13 materials, whereas in the case of the silicoaluminophosphate STA-6, a preliminary screening of some of the achieved SAS-related crystalline samples within the microscope reveals a better crystal homogenization for the selected STA-6 sample (see Figure S8).

The RUB-13_OSDA3 sample crystallizes with an average crystal size of 60-90 nm, and the STA-6_OSDA3 sample shows orthorhombic crystals with average size of 1x4 μm (see FE-SEM images in Figure S11). Elemental analyses of the as-prepared RUB-13_OSDA3 and STA-6_OSDA3 materials indicate that, in both cases, the OSDA3 molecules remain intact within the crystals (see Table S2). Moreover, the calcined RUB-13_OSDA3 and STA-6_OSDA3 samples show micropore volumes of 0.25 and 0.16 $cm^3$/g, respectively, which are comparable to those reported previously in the literature for related materials.(*22, 28*) Chemical analyses indicate that their chemical compositions are almost identical to the initial chemical composition introduced in their corresponding synthesis gels, resulting in a Si/Al ratio of ~16 and a Si/(Al+P) ratio of ~0.13 for the RUB-13_OSDA3 and STA-6_OSDA3, respectively.

The catalytic activity of the RUB-13_OSDA3 and STA-6_OSDA3 materials has been evaluated for the MTO reaction, as before, at 350°C with a WSHV of 0.8 $h^{-1}$. The lower initial methanol conversion values and much higher catalyst deactivation observed with STA-6_OSDA3 (see Figure S15a), is a consequence of the combination of the one-dimensional pore system present within the SAS structure together with the relative large crystal sizes of the STA-6_OSDA3 (1x4μm), which increase the diffusional problems of reactants and products. Nevertheless, it is important to remark that despite the lower initial methanol conversion, the selectivity towards the desired propylene product is very high (~45%, see Figure S15b), suggesting that the SAS-cage would be

adequate to undergo the MTO reaction. The improvement of the diffusion path length by reducing the crystal size or by creating intra-crystalline mesoporosity, should increase the catalyst life.

In the case of the RUB-13_OSDA3 catalyst, it shows an improved catalyst lifetime compared to the standard SSZ-13 zeolite, and a substantially higher propylene selectivity, being the propylene/ethylene ratio (~3.1, see Table 1) much higher than for the CHA-related silicoaluminates (~0.76-0.96, see Table 1). The high selectivity when using the RUB-13_OSDA3 catalyst,(*22, 29*) together with the high specificity of the mimic OSDA3 towards the crystallization of the RTH zeolite, made us to propose that the RTH cavity should better stabilize the pentaMCP$^+$ intermediate than other cage-based small pore zeolites, and then maximize the propylene formation through the paring route compared to other cage-based small pore zeolites. Interestingly, the presence of pentaMCP$^+$ species within the RUB-13_OSDA3 catalyst was undoubtedly observed by $^{13}$C CP-MAS NMR spectroscopy when the MTO reaction was performed using $^{13}$C labelled methanol as substrate (see Figures S20c and S20d).

In the third step of the paring mechanism, there is a ring expansion of the polymethylcyclopentenyl intermediates into a low-alkylated benzene derivative followed by a further alkylation–by two methanol molecules resulting in a high-alkylated benzene intermediate (see INT6 in Figure 1). Thus, we have synthesized an alkylated pyridinium cation as potential mimic of this polyalkylated benzene HP intermediate. As seen in Figure S9, SAPO-18 (AEI structure, 8x8x8-rings) is the preferred crystalline material when OSDA6 is used as organic template. The AEI structure is highly related to CHA, since both present tri-dimensional 8-ring pores with the same framework density (15.1 T atoms per 1000 Å$^3$) and large cavities within their structures. Nevertheless, their cages are different, being the AEI cage basket-shaped and wider at the bottom than the CHA cage, which is more symmetric (see Figure S1).(*30*)

The selected SAPO-18 material (see SAPO-18_OSDA6 in Figure S9) has been characterized by different techniques to unravel its physico-chemical properties. It shows an average crystal size of ~7-10 μm (see SAPO-18_OSDA6 in Figure S11). ICP analysis reveals analogous chemical compositions to those introduced initially in the synthesis gel (see Table S3).

The catalytic activity of the SAPO-18 material synthesized using OSDA6 has been tested for the MTO reaction at 350°C with a WSHV of 0.8 h$^{-1}$. For comparison purposes, a typical SAPO-34 (CHA structure), synthesized using tetraethylammonium (TEA) as OSDA (see experimental section in Supporting Information) has also been tested. The SAPO-34 material shows longer catalyst lifetimes than the SAPO-18_OSDA6 material (~440 versus ~25 min for SAPO-34_std and SAPO-18_OSDA6, respectively, see X95 in Table 1), as could be expected just by taking into account their crystal sizes (~0.5 versus ~7-10 μm for SAPO-34_std and SAPO-18_OSDA6, respectively, see Figure S11). However, when the product selectivities are analyzed, it can be seen that the SAPO-18_OSDA6 sample not only gives a larger $C_3^=/C_2^=$ compared to the SAPO-34_std (~2.0 and ~1.3 for the SAPO-18_OSDA6 and SAPO-34_std, respectively, see Table 1), but also gives a much higher selectivity to $C_4^=$ (~20.0 and ~15.0 for the SAPO-18_OSDA6 and SAPO-34_std, respectively, see Table 1).

It should be taken into account that the paring hydrocarbon pool mechanism can also favor the formation of $C_4^=$ light olefins.(*31*) Therefore, it could be then expected that those zeolite structures that favor the paring route will maximize the $C_3^=/C_2^=$ and $C_4^=/C_2^=$ ratio. Indeed, the two materials giving a higher $C_3^=/C_2^=$, which are RUB-13_OSDA3 and SAPO-18_OSDA6, they also give higher $C_4^=/C_2^=$ compared to typical SSZ-13 or SAPO-34 materials (see Table 1). These results clearly suggest that the particular shape of the RTH and AEI cages should favor the paring hydrocarbon pool compared to another cage-based small-pore zeolite, such as CHA that presents larger and more symmetrical cages, where the side-chain alkylation would more easily occur. In fact, the

outstanding improvement of the catalytic activity observed for SSZ-13_OSDA1b compared to other CHA-related zeolites cannot be attributed to a better stabilization of some of the hydrocarbon pool intermediates within the pairing route, since the $C_3^=/C_2^=$ and $C_4^=/C_2^=$ ratios are comparable to those observed for standard SSZ-13 zeolites. Although we do not have a definitive explanation for this catalytic activity improvement at present, a different distribution of the acid sites within the cavities of the nanosized CHA materials forced by the OSDA1b cation during the synthesis, could explain the remarkable catalytic differences observed.

To get a deeper insight into the preferential stabilization within the zeolites of the different species involved in the paring and side-chain routes, DFT calculations including dispersion interactions were performed on pure silica models of the RTH and CHA cavities (see Figure 4), considering both heptaMB$^+$ and 1,2,2,3,5-pentaMB$^+$ cations as initial hydrocarbon pool species. The calculated interaction energies show a stronger stabilization of all intermediates and transition states involved in the paring route (structures INT0 to INT5 in Figures S2, S3 and S5) in the RTH cavity, with calculated values between -50 and -60 kcal/mol for the first part of the mechanism (Table 2) and slightly lower, from -45 to -55 kcal/mol after split off of the olefin (Table S4), both for heptaMB$^+$ and pentaMB$^+$ HP species. As regards the intermediates involved in the side-chain route, notice that while INT7 participating in the formation of ethylene is also highly stabilized by the RTH cavity, the interaction energy obtained for INT8 is more than 20 kcal/mol lower, reflecting a worse fitting of this bulkier intermediate within the RTH framework, and discarding the formation of propylene via the side-chain pathway in RTH.

The stabilization of cationic species in CHA is weaker than in RTH and depend on the degree of methylation of the HP species. Thus, the structures formed from pentaMB$^+$ cation are stabilized by 40-55 kcal/mol, while the values obtained starting from heptaMB$^+$ are always lower than -50 kcal/mol. It is of particular relevance the low interaction energy values obtained for the heptaMB$^+$

INT0 intermediate and for the two intermediates from the side-chain route, INT7 and INT8, in CHA, all of them around 20 kcal/mol less stable than their corresponding counterparts with pentaMB$^+$ cation as HP. This might be related to the 3-fold symmetry of the CHA cavity, which does not allow the planar and fully methylated heptaMB$^+$ ring to have all the methyl groups pointing to 8MR windows to avoid steric repulsion. Meanwhile, in the case of the less substituted pentaMB$^+$ its smaller size allows this cation to move slightly towards the bottom of the cavity thus maximizing the stabilizing dispersion interactions (see Figure 4). On the other hand, the shape of the RTH cage provides a perfect fit with all structures involved in the paring route, and only the highly substituted INT8 intermediate, generating propylene via the side-chain route, is less stabilized due to steric repulsions.

The differences between RTH and CHA are clearly evidenced in the energy profiles shown in Figure 5. According to the DFT calculations, pentaMB$^+$ cation is similarly stabilized in both zeolites, but its reactivity towards the paring route is low due to the endothermicity of the first step of this pathway producing the bi-cyclic intermediate INT1. Therefore, preferential stabilization of pentaMB$^+$ should direct the reaction towards the side-chain route. Further methylation of pentaMB$^+$ to heptaMB$^+$ cation is difficult in CHA but energetically favored in RTH, so that the whole process following the paring route is favored within RTH framework.

These data also imply that the main species composing the HP in CHA and RTH are different: pentaMB$^+$ cations in the former and heptaMB$^+$ cations in the latter. To evaluate this point, the organic species retained within the SSZ-13_std (CHA) and RUB-13_OSDA3 (RTH) catalysts when the MTO reaction was performed using $^{13}$C labelled methanol as substrate were identified using $^{13}$C CP-MAS NMR spectroscopy (see Figure S20 in the Supporting Information). Different spectra were obtained for the two materials. The spectrum for SSZ-13_std is dominated by two peaks at 125 and 128 ppm associated to -CH$_2$- in benzene rings and two peaks at 19 and 21 that can be assigned

to methyl groups in partially alkylated methylbenzene molecules. The spectrum for RUB-13_OSDA3 (RTH) is more complex and contains, in addition, signals at 132-134 ppm and 11-16 ppm related to fully alkylated benzene and cyclopentadiene rings, as well as a peak at 154 ppm previously assigned to polymethylcyclopentenyl (MPC$^+$) cationic species.(*13*) These data support the preferential stabilization of heptaMB$^+$ and MCP$^+$ species in the RTH cavities, thus favoring the paring route and increasing the selectivity to propylene and butenes.

**CONCLUSIONS**

The results presented here show that the ab-initio design of zeolites for the particular industrially-relevant MTO reaction by properly selecting the OSDA molecules based on the HP intermediates proposed in the literature, is a very attractive methodology not only to design very active and selective MTO catalysts, but also to extract more fundamental knowledge about the very complex reaction mechanism. It is important to remark that the use of the mimics of the paring HP intermediates as OSDAs has resulted in the almost exclusive crystallization of cage-based small pore zeolites, being most of them very active and/or very selective towards the most desired light olefins.

The results obtained with SSZ-13_OSDA1b are especially remarkable since they surpass, by far, the stability of any other CHA reported up to now. The directing effect of the mimic OSDA towards the structure and, probably, towards the location of the active sites under our synthesis conditions helps to further validate our synthesis methodology.(*25*)

This rationalized synthesis approach has been useful for synthesizing zeolites well-adapted for the MTO reaction and could be extended to other chemical processes presenting complex reaction mechanisms, where the ability to design very specific structured catalysts could favor the stabilization of particular intermediates and, consequently, maximize the yield towards the desired products.

**Acknowledgements**

**Figure 1: Proposed hydrocarbon pool mechanisms, including the paring and side-chain routes, for the MTO reaction. Figure adapted from ref. (*10, 13*)**
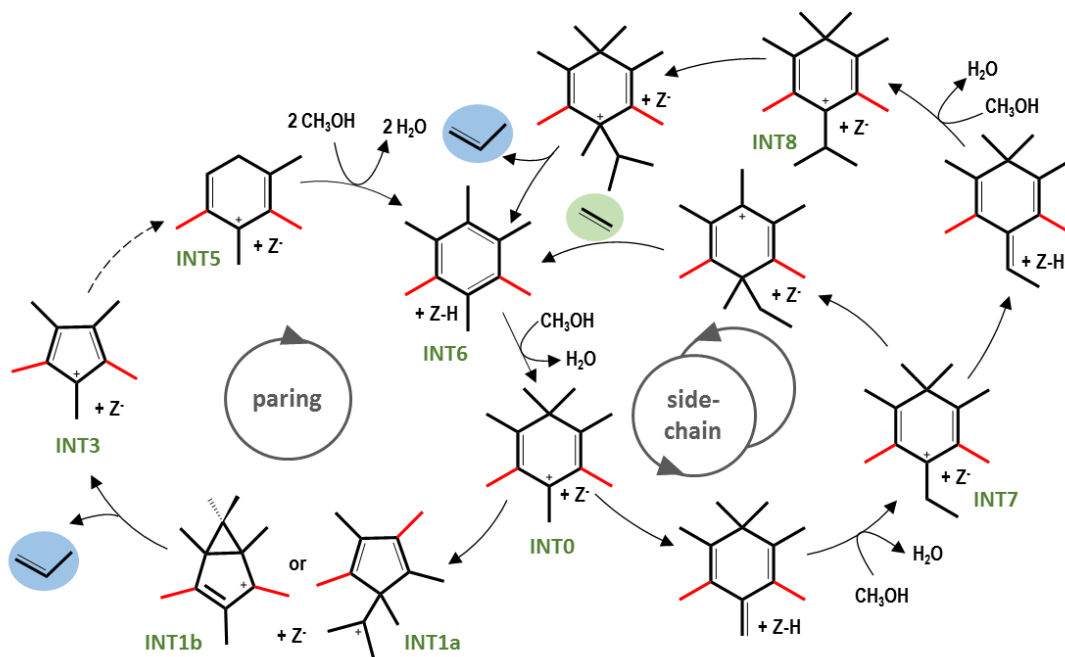
**Figure 2: (a) Proposed OSDA mimics of the different intermediates present in the HP paring route and, (b) zeotypes obtained using these OSDA mimics**
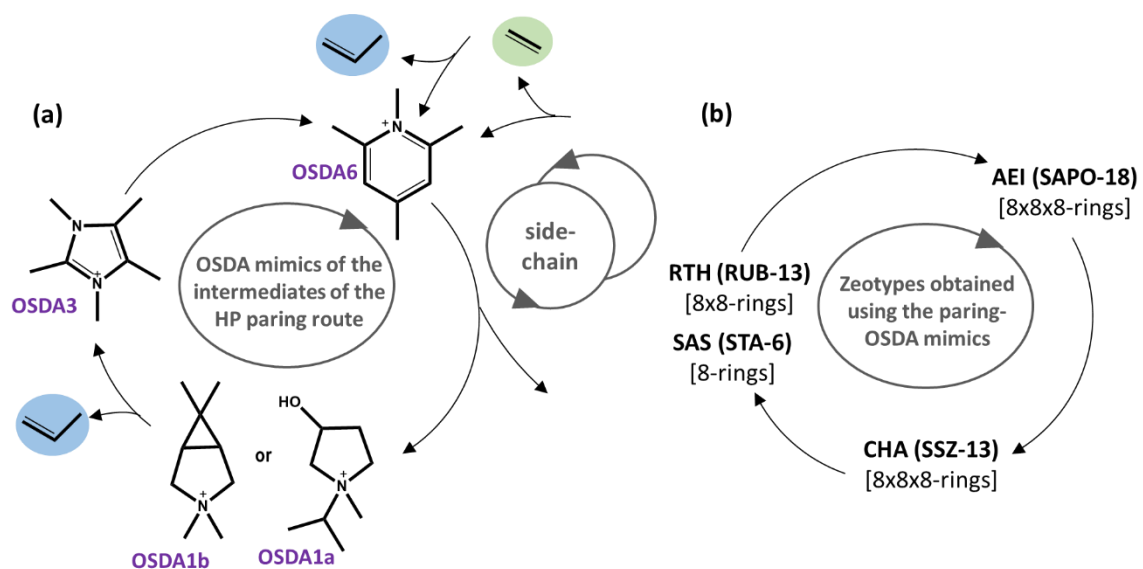
**Figure 3: Comparison of the methanol conversion with TOS for the SSZ-13_OSDA1b, SSZ-13_std, and SSZ-13_nano zeolites reaction (reaction conditions: T=350°C, WHSV=0.8 h$^{-1}$, w$_{cat}$=50 mg)**
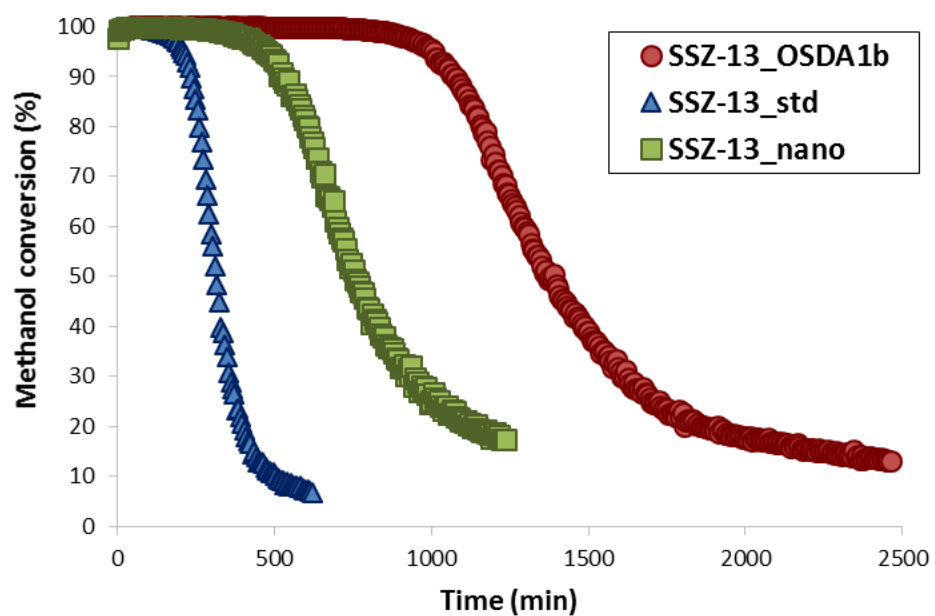
**Figure 4: DFT optimized structures of INT0 species in RTH (top left) and CHA cavity models. INT0 from HeptaMB+ (bottom left) and PentaMB+ (bottom right) in CHA are shown.**
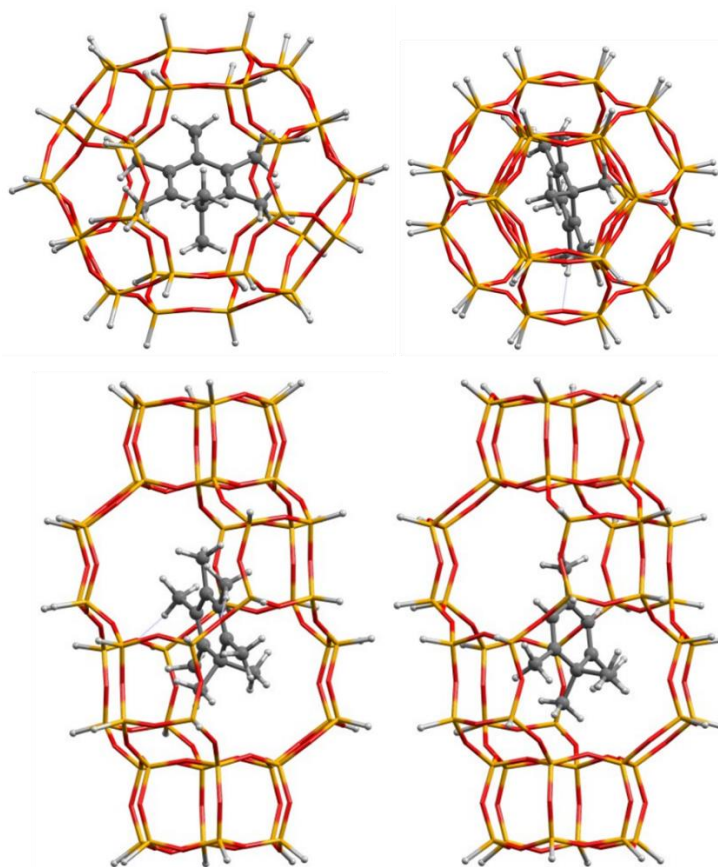
**Figure 5: Calculated energy profile for the paring route in RTH (blue) and CHA (red) models.**
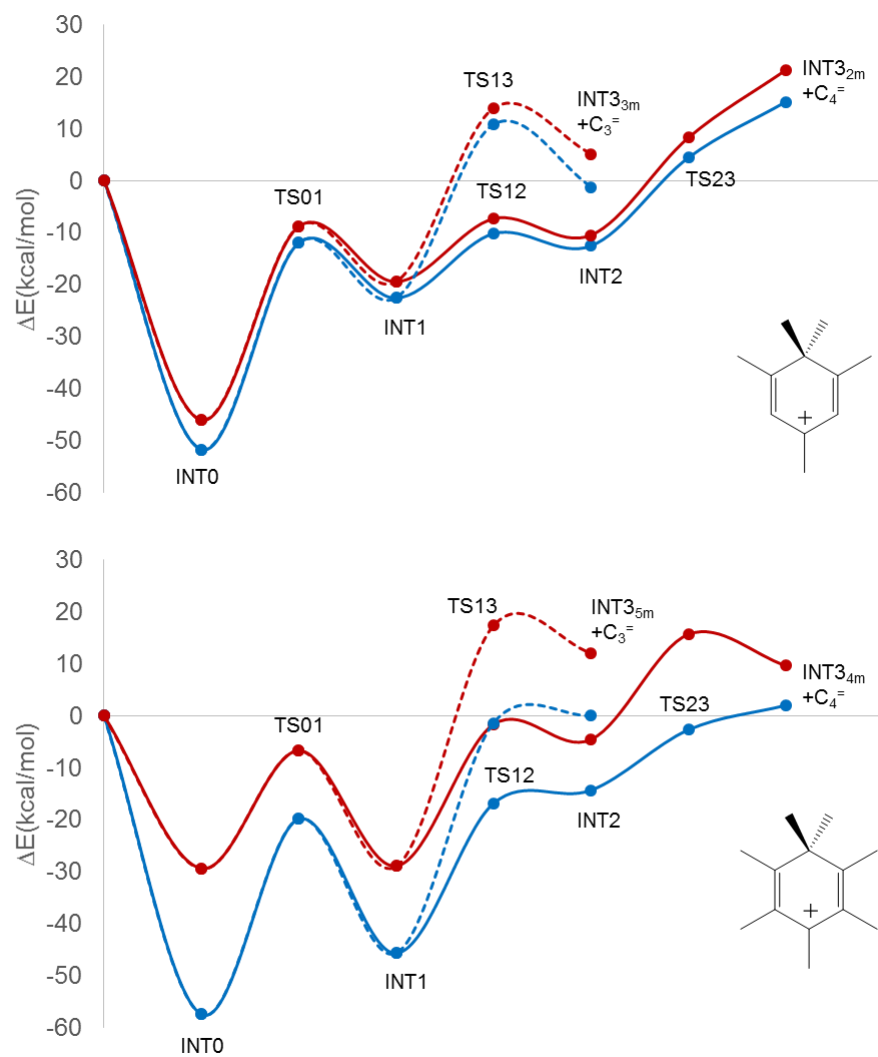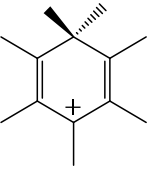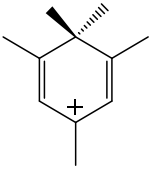
**Table 1: Catalytic properties for the different small pore zeolites for MTO reaction (reaction conditions: T=350°C, WHSV=0.8 h$^{-1}$, w$_{cat}$=50 mg)**

| Sample | Structure | Catalyst lifetime (min) | | Selectivity (%) at X$_{95}$ | | | | |
|---|---|---|---|---|---|---|---|---|
| | | X$_{95}$ | X$_{50}$ | C2$^=$ | C3$^=$ | C4$^=$ | C3$^=$/C2$^=$ | C4$^=$/C2$^=$ |
| SSZ-13_OSDA1a | CHA | 50 | 75 | 40.8 | 37.8 | 5.6 | 0.92 | 0.14 |
| SSZ-13_OSDA1b | CHA | 1005 | 1360 | 45.2 | 34.4 | 10.9 | 0.76 | 0.24 |
| RUB-13_OSDA3 | RTH | 270 | 645 | 14.7 | 45.1 | 24.7 | 3.07 | 1.68 |
| SAPO-18_OSDA6 | AEI | 25 | 90 | 22.2 | 44.5 | 19.9 | 2.00 | 0.89 |
| SSZ-13_std | CHA | 212 | 311 | 39.3 | 37.8 | 15.4 | 0.96 | 0.39 |
| SSZ-13_nano | CHA | 472 | 757 | 43.2 | 37.4 | 14.2 | 0.86 | 0.33 |
| SAPO-34_std | CHA | 440 | 844 | 33.3 | 46.2 | 13.7 | 1.38 | 0.40 |

**Table 2: Stabilization of cationic intermediates and transition states by interaction with RTH and CHA cavity models. DFT calculated interaction energies in kcal/mol.**

| | RTH | CHA | RTH | CHA |
|---|---|---|---|---|
| INT0 | -57,5 | **-29,4** | -51,7 | -46,1 |
| TS01 | -55,1 | -42,1 | -51,9 | -48,7 |
| INT1 | -56,1 | -39,3 | -50,9 | -47,8 |
| TS12 | -54,2 | -39,0 | -51,1 | -48,2 |
| INT2 | -49,8 | -40,1 | -50,1 | -48,1 |
| T23 | -54,5 | -36,1 | -52,3 | -48,5 |
| INT3$_{4m/2m}$+C$_4^=$ | -59,2 | -51,6 | -57,6 | -51,5 |
| TS13 | -59,7 | -40,9 | -56,6 | -53,3 |
| INT3$_{5m/3m}$+C$_3^=$ | -57,5 | -45,5 | -63,3 | -54,9 |
| INT7 | -51,7 | **-26,1** | -42,4 | -48,2 |
| INT8 | **-25,8** | **-29,5** | **-21,2** | -51,5 |

**References:**

1. M. Stocker, Methanol-to-hydrocarbons: catalytic materials and their behavior. *Micropor. Mesopor. Mater.* **29**, 3-48 (1999).
2. P. Tian, Y. Wei, M. Ye, Z. Liu, Methanol to Olefins (MTO): From Fundamentals to Commercialization. *ACS Catal.* **5**, 1922-1938 (2015).
3. S. Ilias, A. Bhan, Mechanism of the Catalytic Conversion of Methanol to Hydrocarbons. *ACS Catal.* **3**, 18-31 (2013).
4. D. Lesthaeghe, V. Van Speybroeck, G. B. Marin, M. Waroquier, Understanding the Failure of Direct C-C Coupling in the Zeolite-Catalyzed Methanol-to-Olefin Process. *Angew. Chem. Int. Ed.* **45**, 1714-1719 (2006).
5. W. Song , J. F. Haw , J. B. Nicholas , C. S. Heneghan, Methylbenzenes Are the Organic Reaction Centers for Methanol-to-Olefin Catalysis on HSAPO-34. *J. Am. Chem. Soc.* **122**, 10726-10727 (2000).
6. S. Svelle *et al.*, Conversion of Methanol into Hydrocarbons over Zeolite H-ZSM-5:  Ethene Formation Is Mechanistically Separated from the Formation of Higher Alkenes. *J. Am. Chem. Soc.* **128**, 14770-14771 (2006).
7. S. Teketel, U. Olsbye, K. P. Lillerud, P. Beato, S. S., Selectivity control through fundamental mechanistic insight in the conversion of methanol to hydrocarbons over zeolites. *Micropor. Mesopor. Mater.* **136**, 33-41 (2010).
8. D. M. McCann *et al.*, A Complete Catalytic Cycle for Supramolecular Methanol-to-Olefins Conversion by Linking Theory with Experiment. *Angew. Chem. Int. Ed.* **47**, 5179-5182 (2008).
9. D. W. K., K. Hemelsoet, M. Waroquier, V. Van Speybroeck, Complete low-barrier side-chain route for olefin formation during methanol conversion in H-SAPO-34. *J. Catal.* **305**, 76-80 (2013).
10. V. Van Speybroeck *et al.*, First principle chemical kinetics in zeolites: the methanol-to-olefin process as a case study. *Chem. Soc. Rev.* **43**, 7326-7357 (2014).
11. C. M. Wang, Y. D. Wang, Z. K. Xie, Verification of the dual cycle mechanism for methanol-to-olefin conversion in HSAPO-34: a methylbenzene-based cycle from DFT calculations. *Catal. Sci. Technol.* **4**, 2631-2638 (2014).
12. B. Arstad, S. Kolboe, The Reactivity of Molecules Trapped within the SAPO-34 Cavities in the Methanol-to-Hydrocarbons Reaction. *J. Am. Chem. Soc.* **123**, 8137-8138 (2001).
13. S. Xu *et al.*, Direct observation of cyclic carbenium ions and their role in the catalytic cycle of th emetahnol-to-olefin reaction over chabazite zeolites. *Angew. Chem. Int. Ed.* **52**, 11564-11568 (2013).
14. J. Chen *et al.*, Elucidating the olefin formation mechanism in the methanol to olefin reaction over AlPO-18 and SAPO-18. *Catal. Sci. Tech.* **4**, 3268-3277 (2014).
15. A. Sassi *et al.*, Methylbenzene Chemistry on Zeolite HBeta:  Multiple Insights into Methanol-to-Olefin Catalysis. *J. Phys. Chem. B* **106**, 2294-2303 (2002).
16. A. Sassi, M. A. Wildman, J. F. Haw, Reactions of Butylbenzene Isomers on Zeolite HBeta: Methanol-to-Olefins Hydrocarbon Pool Chemistry and Secondary Reactions of Olefins. *J. Phys. Chem. B* **106**, 8768-8773 (2002).
17. M. Bjørgen, U. Olsbye, D. Petersen, S. Kolboe, The methanol-to-hydrocarbons reaction: insight into the reaction mechanism from [12C]benzene and [13C]methanol coreactions over zeolite H-beta. *J. Catal.* **221**, 1-10 (2004).

18. M. Zhang *et al.*, Methanol conversion on ZSM-22, ZSM-35 and ZSM-5 zeolites: effects of 10-membered ring zeolite structures on methylcyclopentenyl cations and dual cycle mechanism. *RSC Adv.* **6**, 95855-95864 (2016).

19. Y. Bhawe *et al.*, Effect of Cage Size on the Selective Conversion of Methanol to Light Olefins. *ACS Catal.* **2**, 2490–2495 (2012).

20. N. Martin *et al.*, Nanocrystalline SSZ-39 zeolite as an efficient catalyst for the methanol-to-olefin (MTO) process. *Chem. Commun.* **52**, 6072-6075 (2016).

21. M. Dusselier, M. A. Deimund, J. E. Schmidt, M. E. Davis, Methanol-to-Olefins Catalysis with Hydrothermally Treated Zeolite SSZ-39. *ACS Catal.* **5**, 6078-6085 (2015).

22. T. Yokoi, M. Yoshioka, H. Imai, T. Tatsumi, Diversification of RTH-Type Zeolite and Its Catalytic Application. *Angew. Chem. Int. Ed.* **48**, 9884-9887 (2009).

23. Y. Ji, M. A. Deimund, Y. Bhawe, M. E. Davis, Organic-Free Synthesis of CHA-Type Zeolite Catalysts for the Methanol-to-Olefins Reaction. *ACS Catal.* **5**, 4456-4465 (2015).

24. M. Liu *et al.*, Differences in Al distribution and acidic properties between RTH-type zeolites synthesized with OSDAs and without OSDAs. *Phys. Chem. Chem. Phys.* **16**, 4155-4164 (2014).

25. E. M. Gallego *et al.*, "Ab initio" synthesis of zeolites for preestablished catalytic reactions. *Science* **355**, 1051–1054 (2017).

26. S. I. Zones, *U.S. Patent 4544538, 1985, assigned to Chevron*.

27. Z. Li, M. T. Navarro, J. Martínez-Triguero, J. Yu, A. Corma, Synthesis of nano-SSZ-13 and its application in the reaction of methanol to olefins. *Catal. Sci. Technol.* **6**, 5856-5863 (2016).

28. R. Martínez-Franco, A. Cantin, M. Moliner, A. Corma, Synthesis of the Small Pore Silicoaluminophosphate STA-6 by Using Supramolecular Self-Assembled Organic Structure Directing Agents. *Chem. Mater.* **26**, 4346-4353 (2014).

29. J. E. Schmidt, M. A. Deimund, D. Xie, M. E. Davis, Synthesis of RTH-Type Zeolites Using a Diverse Library of Imidazolium Cations. *Chem. Mater.* **27**, 3756–3762 (2015).

30. M. Moliner, C. Franch, E. Palomares, M. Grill, A. Corma, Cu–SSZ-39, an active and hydrothermally stable catalyst for the selective catalytic reduction of NOx. *Chem. Commun.* **48**, 8264-8266 (2012).

31. C. M. Wang, Y. D. Wang, H. X. Liu, Z. K. Xie, Z. P. Liu, Theoretical insight into the minor role of paring mechanism in the methanol-to-olefins conversion within HSAPO-34 catalyst. *Micropor. Mesopor. Mater.* **158**, 264-271 (2012).